https://doi.org/10.22226/2410-3535-2020-2-189-194 PACS: 62.20.Qp, 68.35.Np, 68.47.Fg, 61.10.Nz

Photon treatment effect on the hardness and surface adhesion of thermoelectric legs based on Bi_2Te_3-Bi_2Se_3 and Bi_2Te_3-Sb_2Te_3 systems

E. K. Belonogov[1,2], V. A. Dybov[1], A. V. Kostyuchenko[1], S. B. Kushev[1], D. V. Serikov[†,1], S. A. Soldatenko[1,3], M. P. Sumets[2]

[†]dmitriy.tut@mail.ru

[1]Voronezh State Technical University, 14 Moskovskij Av., Voronezh, 394000, Russia
[2]Voronezh State University, 1 Universitetskaya Sq., Voronezh, 394000, Russia
[3]Military Aviation Engineering University, 54A Starykh Bolshevikov St., Voronezh, 394064, Russia

In this work, the composition, morphology and mechanical properties of the surface of semiconductor thermoelectric legs before and after the pulsed photon treatment were studied. The n-type (Bi_2Te_3-Bi_2Se_3) and the p-type (Bi_2Te_3-Sb_2Te_3) legs fabricated by a hot pressing method were treated using a special technique, including mechanical polishing, pulsed photon irradiation with xenon lamps and electrochemical etching. The pulsed photon treatment significantly enhanced mechanical properties and adhesion hardness of the thermoelectric legs. The mechanical polishing followed by the pulsed photon treatment increased the adhesion of the barrier and commutation Mo/Ni layers three- and twofold for the n-type and p-type legs, respectively. The pulsed photon treatment stimulated local recrystallization of the surface defect layer up to 100 – 200 nm in-depth under an effective temperature of about 800 K in the near-surface layer of branches. Besides, the pulsed photon treatment increased the surface hardness of the Bi_2Te_3-Bi_2Se_3 system by 1.2 times. The surface modification of thermoelectric legs through the pulsed photon treatment did not decline the barrier properties of the Mo-layer in Ni-Mo-Bi_2Te_3 + Bi_2Se_3 heterostructures.

Keywords: pulsed photon treatment, bismuth telluride, surface modification, thermoelectric leg, phase composition, adhesion strength.

УДК: 537.323, 539.536, 539.612

Влияние фотонной обработки на твердость и адгезионные свойства поверхности термоэлектрических ветвей на основе твердых растворов Bi_2Te_3-Bi_2Se_3 и Bi_2Te_3-Sb_2Te_3

Белоногов Е. К.[1,2], Дыбов В. А.[1], Костюченко А. В.[1], Кущев С. Б.[1], Сериков Д. В.[†,1], Солдатенко С. А.[1,3], Сумец М. П.[2]

[1]Воронежский государственный технический университет, Московский пр-т, 14, Воронеж, 394000, Россия
[2]Воронежский государственный университет, Университетская пл., 1, Воронеж, 394000, Россия
[3]Военно-воздушная академия им. профессора Н. Е. Жуковского и Ю. А. Гагарина, ул. Старых большевиков, 54А, Воронеж, 394064, Россия

В данной работе представлены результаты исследований состава, механических свойств и морфологии поверхности полупроводниковых термоэлектрических ветвей до и после импульсной фотонной обработки. Ветви получали методом горячего прессования порошка теллурида висмута, имеющего n- (Bi_2Te_3-Bi_2Se_3) и p-тип (Bi_2Te_3-Sb_2Te_3) проводимости, и подвергали специальным обработкам, механической полировке, электрохимическому травлению и импульсному облучению фотонами ксеноновых ламп. Импульсная фотонная обработка увеличивает твердость

и повышает адгезионную прочность поверхностных слоев термоэлектрических ветвей. Механическая полировка с последующей импульсной фотонной обработкой увеличивает адгезию барьерных и коммутационных слоев Mo/Ni в три раза для ветвей n-типа и в два раза для ветвей p-типа проводимости. Импульсная фотонная обработка стимулирует локальную рекристаллизацию поверхностного дефектного слоя на глубину до 100 – 200 нм, поскольку при данных режимах обработки в приповерхностном слое ветвей возникает эффективная температура ~800 K. Кроме того, такая обработка приводит к повышению твердости поверхностного слоя ветвей системы Bi_2Te_3-Sb_2Te_3 в 1.2 раза. Барьерные функции слоя молибдена после импульсной фотонной обработки не нарушаются.

Ключевые слова: импульсная фотонная обработка, теллурид висмута, модификация поверхности, термоэлектрическая ветвь, фазовый состав, адгезионная прочность.

1. Introduction

The increase in the efficiency of thermoelectric devices is of great interest in alternative energy harvesting. There are two approaches to attain this increase: 1) the development of new thermoelectric materials and technologies; 2) the fabrication of highly reliable metal-semiconductor commutation contacts. The first approach was the most efficient in the last decade, whereas the second one was not so promising. Nowadays, the adhesion strength of commutations is the main technological problem [1, 2].

The bismuth telluride (Bi_2Te_3)-based solid solutions containing Se and Sb can be used for the fabrication of thermoelectric legs effectively operating in a temperature range of 373 – 523 K [3]. These legs can be either n- or p-type conductivity and commute through the conducting ports (Cu, Ag and Al). Various compositions, such as Sn-Ag, Sn-Ag-Bi-Cu, Sn-Bi, and Bi-Sb, are used for the soldering of the semiconductor and the commutating port. Thin conducting barrier layers (Ni, Mo, Ni-P, Co, Ta-Si-N) are deposited onto a semiconductor leg surface to prevent interdiffusion of elements between the solder and the conducting port. These layers provide low diffusion mobility of the elements along with high adhesion to the legs and solder material [4]. The required resistivity and adhesion strength of the barrier metallization have to be less than 10^{-9} Ohm · m^2 and at least 8 N/mm^2 respectively [5].

The degradation of the commutation contacts as a part of Bi_2Te_3-based thermoelectric elements is originated from the low material strength and weak adhesion between a barrier metallization layer and semiconductor legs [6]. It can be improved through the modification of subsurface layers in the semiconductor legs [7]. Currently, the leg surfaces are modified by mechanical and chemical polishing [8] Bi_2Te_3, and its alloys have been demonstrated. In designing high-performance thermoelectric devices, variations in the thermal and electrical contact resistances due to interfacial effects between the nanostructured alloy and the metallic electrodes remain a significant issue. Smooth scratch-free surfaces should provide a baseline for contact resistance studies. In this paper, the root mean square roughness over a 10 μm^2 of nanostructured bismuth tellurium based alloys was reduced from 133 nm to 1.9 nm by a procedure consisting of electrolysis, mechanical polishing, and chemical mechanical polishing (CMP, electroerosion cutting [9], and depositing the Bi_2Te_3 layers [10]. However, this problem is not resolved yet.

The pulsed photon treatment (PPT) by high-power xenon lamp irradiation is an innovative surface modification [11]. This method has the following advantages: treatment of wide areas, simple and low-cost equipment, a very fast process (1 – 3 sec). The PPT does not change the structure, elemental and phase composition, bulk physical and chemical properties under irradiation of the subsurface layer (few nanometers thick). The present work aims to reveal the laws of the phase and structural transformations occurring in the subsurface layer of the thermoelectric Bi_2Te_3-Bi_2Se_3 (n-type) and Bi_2Te_3-Sb_2Te_3 (p-type) legs after PPT. The mechanical and adhesion properties of the modified surface are studied.

2. Material and methods

Semiconductor legs based on the Bi_2Te_3-Bi_2Se_3 (n-type) and Bi_2Te_3-Sb_2Te_3 (p-type) solid solutions were fabricated under the following technological regime: cold pressing of a powder sample of a required composition; static hot pressing (T = 670 K) in an Ar environment; thermal annealing of as-prepared samples at a temperature of 570 K in an Ar atmosphere for 24 hours; cutting the samples with a diamond disc to obtain the desired legs.

To study the PPT effect on the modification of semiconductor surfaces, we carried out a comparative study of the hardness and adhesive properties of the surfaces modified by other conventional techniques. The following three methods were applied to the semiconductor legs prior to the deposition of Mo and Ni films: mechanical polishing (MP); mechanical polishing followed by the PPT (MP + PPT); mechanical polishing followed by electrochemical polishing (MP + ECP).

The MP was performed using a grinding disc with the SiC abrasive paper (from P2000 to P5000) attaining a mirror surface, followed by ultrasonic cleaning in deionized water. After that, some samples were treated by PPT, while others were under ECP.

PPT was carried out by xenon lamps (in the wavelength range ranging from 0.2 to 1.2 μm) in an Ar atmosphere. The following two irradiation regimes were used: double exposure with pulses of 10^{-2} sec during 0.8 and 1.0 seconds for the p- and n-type legs, respectively. These regimes correspond to the energies supplied to the sample equaled to $E_r \sim 80$ J/cm^2 and ~125 J/cm^2, respectively. The regimes were designed based on our previous investigations [12].

For ECP, the sample was placed in an electrolyte (anode) between two graphite cathodes. One liter of deionized water-based electrolyte contained NaOH (85 g) and $H_2C_4H_4O_6$ (60 g). The ECP process was performed during 1 min at a current density of 120 mA/cm^2 and voltages of 9 and 12 V for p- and n-type materials, respectively. Finally, the legs were cleaned in deionized water.

Ni was used as a commutation layer, whereas Mo served as a barrier layer. The Mo and Ni layers were deposited onto the semiconductor legs by the magnetron sputtering method (RFMS, UVN-74M) in an Ar gas environment under a working pressure of $4.2 \cdot 10^{-4}$ mm Hg. The legs were heated up to 470 K with UV lamps. The magnetron power was 900 and 600 W, providing a condensation rate of 3.3 and 1.8 nm/min for Mo and Ni targets, respectively. The thickness of each layer was 250 nm.

The phase composition and structure were studied by X-ray diffractometry (Bruker D2 Phaser). The average size of the coherent scattering region (CSR) was determined through the Selyakov-Scherer method using the Highscore Plus software (Pan Analitical). A NIST SRM-1976 sample was used as an instrumental standard. The surface morphology was studied using atomic force microscopy (AFM, NT-MDT Solver P47) and scanning electron microscopy (SEM, JEOL JSM6380LV devices). The hardness of the samples was studied by the nano-indentation method (Nano Hardness Tester (CSM Instruments)) with the Bercovich's diamond indenter. The highest loading magnitude was 10.0 and 200 mN at a rate of 15 and 300 mN/min, respectively. The hardness (Mayer's scale) and Young modulus magnitudes for the surface layers were determined by the Oliver-Pharr method according to GOST P 8.748-2011. The obtained results were analyzed using the "Indentation" software. The adhesion measurements between the coatings and the legs were conducted by a shear testing method using the RPM-10MG4 tensile testing machine at a loading transverse rate of 1.0 mm/min. The adhesion magnitude was calculated as $R = P/F$, where P is the maximum loading, F is the glued area.

3. Results and discussion

3.1. N-type semiconductor legs

3.1.1. Phase composition

Fig. 1. shows the XRD patterns characterizing the phase composition of the subsurface layers associated with n-type semiconductor legs before and after various surface treatments (inset (A) shows an enlarged plot of 01.5 peaks).

The XRD pattern of as-prepared samples (spectrum 1) contains reflexes attributed only to the Bi_2Te_2Se phase with the rhombohedral lattice ($R\bar{3}m$) [13]. The relatively high intensity of both (00.6) and (00.15) peaks indicates the existence of <0001> texture.

It follows from Fig. 1, that MP, PPT, and ECP have no effects on the phase composition of the subsurface layers. However, the intensity and width of all peaks in Fig. 1 for the samples with modified surfaces differ from those for the as-prepared samples. MP reduces the intensities and increases the width of (00.6) and (00.15) reflexes. This effect can be explained by the formation of defects and the high strength in the subsurface layers due to deformation. In contrast, the width of the diffraction peak decreases for the samples after ECP due to the removal of the deformed layer, resulting from MP. The redistribution of 00.6 and 00.15 peak intensities along with the width decreasing for the samples after PPT are originated from the recrystallization process occurring in the subsurface layer. This process leads to decreasing strength and the formation of arbitrarily oriented grains because the effective temperature rises to ~800 K in the subsurface layer under these PPT regimes [12].

3.1.2. Mechanical properties

When analyzing nanoindentation, it is necessary to take into account the following: hardness (H) characterizes the elastic-plastic properties of a layer with a thickness close to the indenter penetration depth (0.2 – 0.4 μm under an indenter load (F) of 10 mN and 3.54.0 μm under $F = 200$ mN). Young›s modulus (E) describes the elastic properties of a layer with a thickness of more than an order of magnitude greater than the indenter penetration depth.

An increase in H in the surface layer under a load of 10 mN (see Table 1) in the case of MP can be explained by the formation of a dispersed grain structure resulting in the plastic deformation of the surface layer up to 0.5 μm thick. A decrease in H under $F = 200$ mN can be addressed to the lower hardness of underlying layers with a coarse-grained structure and the [0001] texture.

The observed decrease in E is originated from the occurrence of microcracks between grains under MP, which is confirmed by SEM [12].

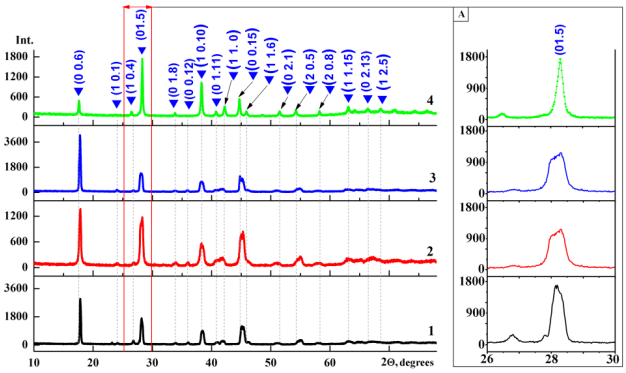

Fig. 1. (Color online) XRD patterns of the studied legs based on the Bi_2Te_3-Bi_2Se_3 solid solutions (n-type) before (1) and after MP (2), MP ECP (3), MP PPT (4) (inset (A) shows an enlarged plot of 01.5 peaks).

Table 1. Hardness (H) and Young's modulus (E) of the surface layer for an n-type semiconductor legs after various treatments.

Surface treatment	Loading			
	F=10 mN		F=200 mN	
	H, GPa	E, GPa	H, GPa	E, GPa
As-prepared sample	1.1	29.7	0.9	29.5
MP	1.3	26.9	0.7	21.6
MP + PPT	1.3	31.2	0.9	32.8
MP + ECP	1.0	21.9	0.6	21.7

The PPT of mechanically polished legs leads to an increase of H under $F=200$ mN due to the formation of a grained structure with an arbitrary crystallite orientation in the surface layer up to few microns thick. The E increases due to the coagulation and redistribution of micropores in a surface region of legs. [12].

Thus, the H and E magnitudes, characterize the elastic properties of layers consisting of flat [0001]-textured micrograins, regardless of the loading.

3.1.3. Adhesion properties

The commutation, barrier and subsurface layers of semiconductor samples contain only pure metallic and Bi_2Te_2Se phases. Consequently, the chemical interaction does not occur at the Bi_2Te_2Se/Mo/Ni heterointerfaces after deposition of Mo and Ni onto a semiconductor at a temperature of 470 K by the RFMS method.

It was revealed through a shear test, that the only Bi_2Te_2Se phase exists in the area of metallization detachment. Therefore, the heterostructure is destroyed along the interface (adhesion disruption) or in the bulk of the semiconductor (cohesion disruption). Table 2 summarizes the adhesion magnitudes for coatings and the disruption types for Bi_2Te_2Se/Mo/Ni heterostructure, obtained through AFM investigation.

When the coatings are deposited onto the as-prepared (non-treated) surface, adhesion is minimal due to the contamination and high concentration of defects (cracks, pores) in a subsurface layer.

The adhesion of legs after MP and MP + PPT exceeds fourfold that for the as-prepared samples. This result correlates with indentation data, resulted from the presence of a highly-dispersed hardened layer with the grained structure.

The adhesion of coatings after ECP is two times higher than that for the non-treated legs. The adhesion increase occurs due to the presence of elongated cavities along the grain boundaries. At the same time, the adhesion of coatings and legs treated by ECP is considerably weaker compared to that for the legs after MP and MP + PPT. This result is clear because disruption occurs easily along the cleavage planes (0001) in the bulk of Bi_2Te_2Se. The large [0001]-textured grains, existing in a subsurface layer after ECP decrease the shearing strains. This effect provokes the easier disruption of the subsurface layer compared to that with small arbitrary oriented grains.

3.2. P-type semiconductor legs

3.2.1. Phase composition

Fig. 2. demonstrates the XRD patterns of the surface layers for p-type semiconductor legs before and after various surface treatments (inset (B) shows an enlarged plot of 01.5 peaks).

The XRD pattern of as-prepared legs (curve 1 in Fig. 2.) contains the reflexes attributed to the rhombohedral lattice of $Bi_{0.4}Sb_{1.6}Te_3$ ($R\bar{3}m$) [13]. The relatively high intensity of (00.6) peak indicates the existence of the <0001>-texture. Besides, some reflections correspond to the hexagonal cell of Te.

Table 2. The adhesion magnitudes and the disruption type for Bi_2Te_2Se/Mo/Ni heterostructures.

Surface treatment	R_{shear}, MPa	Disruption type
As-prepared sample	1.3	Cohesion: in the bulk of a semiconductor
MP	5.6	Hybrid: in the bulk of a semiconductor and along the semiconductor/metal interface
MP + PPT	5.5	Adhesion: along the semiconductor/metal interface
MP + ECP	2.3	Cohesion: in the bulk of a semiconductor

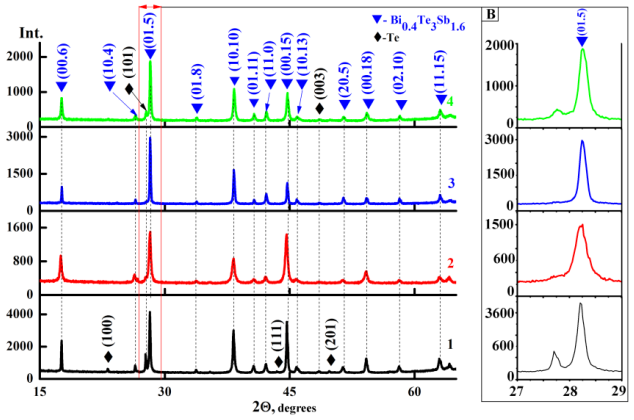

Fig. 2. (Color online) XRD patterns of the legs based on the Bi_2Te_3-Sb_2Te_3 solid solutions (p-type) before (1) and after MP (2), MP + ECP (3), MP + PPT (4) ((B) inset shows an enlarged plot of 01.5 peaks).

The segregation of Te phase in the subsurface layer under thermal annealing is caused by the temperature dependence of a homogeneity area in the phase diagram of Bi_2Te_3 [14]. In a temperature range of 670 – 858 K, the homogeneity area narrows monotonically. Consequently, the excessive Te segregates at the grain boundaries of Bi_2Te_3 under thermal annealing of a homogeneous composition in this temperature range. Under relatively fast cooling, occurring in a surface area, the Te inclusions does not dissolve entirely (frozen condition).

As seen from Fig. 2, MP increases the width of diffraction peaks and decreases the (00.6) peak intensity. This data proves that the grain size (40 nm) decreases in the surface layer and the existing texture becomes weaker. Alternatively, the diffraction peak broadening can be originated from stress, occurring in the surface layers due to deformation.

The XRD patterns of the studied legs after MP and MP + ECP demonstrate reflexes, attributed to the $Bi_{0.4}Sb_{1.6}Te_3$ phase. Thus, Te is removed from the surface during these treatment processes. The width peak decrease attributed to $Bi_{0.4}Sb_{1.6}Te_3$ (curve 3 in Fig. 2), indicates that a hardened layer occurred under MP is removed by ECP treatment. The grain

size for MP + ECP samples, estimated from the peak width of 01.5, is 85 nm. The 01.5 peak was selected as the most intense one to minimize the background influence and calculate the peak intensity (and half maximum).

After MP + PPT, the slight peak narrowing was observed along with reflexes attributed to Te. Similar to n-type legs, these changes are originated from the recrystallization processes taking place at the leg surfaces due to an effective temperature of 800 K, produced by PPT. The Te formation in the surface area after PPT is caused by temperature dependence of homogeneity area in the phase diagram of Bi_2Te_3 [14].

3.2.2. Mechanical properties

The hardness *H* and Young's modulus *E* of semiconductor p-type legs after various treatments are given in Table 3.

The results given in Table 3 for MP and MP + ECP are analogous to those for n-type legs (see Table 2.). Consequently, the magnitudes of *H* and *E* decrease due to the removal of a deformed surface layer in the process of ECP.

Similarly to n-type legs, MP + PPT lead to recrystallization and the formation of surface layers with arbitrary grain orientation. The layer thickness exceeds the indenter penetration depth, because the magnitudes of *H* are close for two loadings given in Table 3. Unlike n-type legs, the *H* and *E* magnitudes decrease compared to those for the mechanically polished legs resulting from the formation of closed porosity in a re-crystallized layer. As followed from the XRD analysis, this layer is formed due to the re-distribution of Te atoms in the form of a separate phase.

3.2.3. Adhesion properties of the legs

With the use of XRD diffraction method, three phases (Mo, Ni, and $Bi_{0.6}Sb_{1.6}Te_3$) and four phases (Mo, Ni, $Bi_{0.6}Sb_{1.6}Te_3$, and Te) were identified for the studied heterostructures after MP + ECP and MP + PPT respectively. Therefore, metallization of semiconductor legs does not trigger chemical interactions and phase formation at the semiconductor/metal interface.

A shear test revealed that the only the $Bi_{0.6}Sb_{1.6}Te_3$ phase is observed on the torn surface. Thus, the heterostructure is disrupted along the semiconductor leg-metallization interface (the adhesion disruption) or in the volume of a semiconductor (the cohesion disruption). Besides, the study of Mo surfaces revealed the $Bi_{0.6}Sb_{1.6}Te_3$ phase along with pure metal, which proves the dual disruption mechanism.

The surface adhesion magnitudes and disruption types for the studied heterostructures, derived from AFM investigations of the surface torn out from the coating are given in Table 4.

For the coatings deposited onto the non-modified leg surface, the adhesion magnitude is relatively low and ranges from 1.2 to 2.1 MPa. The reason for this is a large number of defects (pores and cracks) in the surface layer of the semiconductor leg.

As seen from Table 4, the polishing of the p-type legs doubles the adhesion of Mo/Ni barrier layers, resulting from a decrease in the number of defects and hardening of the surface layer.

Table 3. The hardness (*H*) and the Young's modulus (*E*) of a surface layer for the p-type semiconductor legs after different treatments.

Surface treatment	Loading			
	F=10 mN		*F*=200 mN	
	H, GPa	*E*, GPa	*H*, GPa	*E*, GPa
As-prepared sample	1.3	33.5	1.0	31.2
MP	1.5	36.8	0.8	29.7
MP + ECP	1.0	28.6	0.7	25.9
MP + PPT	1.1	31.8	1.0	29.2

Table 4. The adhesion magnitudes and disruption types for semiconductor-metallization heterostructures.

Surface treatment	R_{shear}, MPa	Disruption type
As-prepared	1.2 – 2.1	Cohesion: in the bulk of a semiconductor
MP	2.3 – 2.7	Hybrid: in the bulk of a semiconductor and along the semiconductor/metal interface
MP + ECP	1.2 – 3.7	1.2 MPa - cohesion: along the cleavage planes in a semiconductor; 3.7 MPa – hybrid: in the bulk of a semiconductor and along the semiconductor/metal interface
MP + PPT	2.3 – 3.9	Hybrid: in the bulk of a semiconductor and along the semiconductor/metal interface

After MP + ECP, low adhesion (~1.2 MPa) was observed for the samples whose surface layers (0.1 mm thick) were removed by MP. The textured large-grain layers with the cleavage planes parallel to the surface were observed on the leg surfaces. As a result, a disruption along the cleavage planes in the semiconductor bulk occurs (cohesion mechanism). The coating-to-leg adhesion after ECP was observed only when a relatively thick layer (100 – 200 μm) was removed by mechanical polishing. In this case, the defect layer, deformed by pressing, is removed entirely by MP, and the subsequent ECP improves the morphology. Metallization is deposited onto a smooth defect-free surface, and the disruption occurs in the semiconductor bulk or along the semiconductor/metal interface.

The adhesion magnitude of 2.3 MPa corresponds to the legs after their single PPT. Double PPT, performed after mechanical polishing, increases adhesion up to 3.9 MPa. In both cases, the disruption occurs in the semiconductor bulk and parallel to the semiconductor/metal interface.

Conclusions

In the present work, we demonstrated the efficiency of PPT in terms of increasing the surface hardness and adhesion strength of semiconductor legs based on Bi_2Te_3-Bi_2Se_3 (n-type) and Bi_2Te_3-Sb_2Te_3 (p-type) solid solutions. The mechanical polishing of thermoelectric legs followed by PPT increased by 3 – 4 times (for n-type legs) and 2 times (for p-type legs) the adhesion of barrier and commutation Mo/Ni layers. PPT stimulated local recrystallization of the defect layer 100 – 200 nm in-depth and increased by 1.2 times the surface hardness for n-type legs.

Acknowledgments. This work was supported by the Ministry of Education of the Russian Federation (the Russian Federation government decree: Agreement #03.G25.31.0246) and was performed using the scientific equipment of the Borisov's Center for Collective Use of the Voronezh State Technical University.

References

1. X. Zhu, L. Cao, W. Zhu, Y. Deng. Adv. Mater. Interfaces. 5 (23), 1801279 (2018). Crossref
2. Y. I. Shtern, R. E. Mironov, M. Y. Shtern, A. A. Sherchenkov, M. S. Rogachev. Acta Phys. Polon. A. 129 (4),785 (2016). Crossref
3. W. Xie, X. Tang, Y. Yan, Q. Zhang, T. M. Tritt. Appl. Phys. Lett. 94, 102111 (2009). Crossref
4. W. Brostow, T. Datashvili, H. E. Hagg Lobland, T. Hilbig, L. Su, C. Vinado, J. White. J. Mater. Res. 27, 2930 (2012). Crossref
5. M. Y. Shtern, Y. I. Shtern, A. A. Sherchenkov. Russ. Microelectron. 41 (7), 393 (2012). Crossref
6. N. Y. C. Yang, A. M. Morales. Metallurgy, Thermal Stability, and Failure Mode of the Commercial Bi-Te-Based Thermoelectric Modules. Albuquerque, NM, and Livermore, CA (2009). Crossref
7. G. C. Dannangoda, C. Key, M. Sumets, K. S. Martirosyan. J. Electron. Mater. 47, 5800 (2018). Crossref
8. H.-P. Feng, B. Yu, S. Chen, K. Collins, C. He, Z. F. Ren, G. Chen. Electrochim. Acta. 56, 3079 (2011). Crossref
9. A. I. Voronin, V. T. Bublik, N. Y. Tabachkova, Y. M. Belov, J. Electron. Mater. 40, 794 (2011). Crossref
10. I. S. Virt, T. P. Shkumbatyuk, I. V. Kurilo, I. O. Rudyi, T. Y. Lopatinskyi, L. F. Linnik, V. V. Tetyorkin, A. G. Phedorov. Semiconductors. 44, 544 (2010). Crossref
11. V. M. Ievlev. Russ. Chem. Rev. 82, 815 (2013).Crossref
12. E. Belonogov, V. Dybov, A. Kostyuchenko, S. Kushev, D. Serikov, S. Soldatenko. J. Surf. Investig. X-Ray, Synchrotron Neutron Tech. 13, 371 (2019). Crossref
13. ICDD PDF-2, Release, No.01-072-1836 (2004).
14. P. R. S. H. Okamoto. Binary Alloy Phase Diagrams, 2nd ed. ASM International, Materials Park, Ohio, USA (1990) 1129 p.